Multi-phase flow in single fracture

Sumihiko Murata, Daisuke Fukahori, Tsuyoshi Ishida
Graduate School of Engineering, Kyoto University
Takashi Akai
Japan Oil, Gas and Metals National Corporation (JOGMEC)

Abstract

For the successful development of a fractured reservoir, it is important to estimate the multi-phase fluid flow behavior in a single fracture. However, how the wettability of the fracture surfaces, the interfacial tension between water and oil, and the geometries of the fracture surfaces affect the multi-phase flow behavior is not understood sufficiently well.

In this study, in order to understand these problems, we try to conduct a visualization experiment of water flooding in a single fracture, and then we try to simulate the multi-phase flow behavior observed in the experiment by using the lattice Boltzmann method (LBM). Consequently, we have gained a good understanding of the multi-phase flow behavior in a single fracture, and we can estimate the effect of the wettability and the interfacial tension on the multi-phase flow behavior.

1. Introduction

To estimate the multi-phase fluid flow through a fracture is important for the successful development of fractured oil and gas reservoirs and for environmental problems, especially for the geological sequestration of CO_2. This is because the reservoir fluids or the injected CO_2 mainly flow through fractures since the fractures have higher permeability than the matrix of rock masses.

Generally, the fracture permeability has been estimated by the cubic law, that is, the volumetric flow rate in a fracture is directly proportional to the cubic of its aperture. This law is valid for the laminar flow between two perfectly smooth parallel plates. However, the fractures have complicated rough surfaces. This makes the fluid flow through them anisotropic and their permeability deviate from the cubic law. In addition, the two straight lines satisfying the relation of $k_{r,nw} + k_{r,w} = 1$ have been used for the fracture relative permeability curves based on the experimental works by Romm (1966), where $k_{r,nw}$ and $k_{r,w}$ are the relative permeability of the non-wetting phase and wetting phase respectively. This type of the relative permeability curves physically means that the each phase flows in its own flow path without interference. But, some theoretical or experimental work and some numerical simulations to the two-phase flow in a single fracture has shown that the each phase flows with strong phase interference[1-4]. However, these works are not sufficient to understand the phase interference flow behavior for the correct estimation of the fracture relative permeability. Therefore, additional detail research on the multi-phase flow in a single fracture must be performed.

In this study, we try to conduct a visualization experiment of water flooding in a single fracture, and then we try to simulate and to estimate the relative permeability to the single fracture models having complex surface geometry by performing two-phase flow simulations using the lattice Boltzmann method (LBM). Moreover, we investigate the effect of the wettability and the interfacial tension on the multi-phase flow behavior and the relative permeability by the LBM two-phase flow simulations.

2. Visualization experiment of water flooding

2.1. Specimen for the visualization experiment

It has been shown that the topography of a fracture surface is a self-affine fractal and the power spectral density function of fracture surface profiles, $G(f)$, shows a decaying power law that can be described as

$$G(f) = Cf^{-(5-2D)} \tag{1}$$

where D is the fractal dimension; C is a constant; f is the spatial frequency [5, 6]. The two meeting surfaces of a single fracture correlate each other in lower spatial frequency band and do not correlate in higher spatial frequency band. By this frequency dependent correlation, the meeting fracture surfaces interlock with each other and the aperture distribution is formed.

In order to numerically generate the two meeting fracture surfaces, we used the Glover's method [7]. The fractal dimension and roughness of generated fracture surface can be set by changing the slope and intersection of the decaying power law respectively on the double logarithmic plot. Here, we set the fractal dimension 2.2 and the roughness 0.254mm in root mean square height. The numerically generated single fracture whose size is 50mm x 50mm is shown in Fig. 1. The black areas in this figure are contact areas.

For the visualization experiment of water flooding, we prepared a transparent specimen containing a single fracture by the following procedures. Firstly, we carved the two meeting fracture surfaces separately on a modeling wax using a numerical controlled (NC) modeling machine, PNC-300G produced by Roland DG. The numerical height data comes from the above mensioned numerically generated fracture. Secondly, we individually copied the two carved surfaces with white silicon gum and transparent acrylic resin. Finally, we mated them together. By using silicon gum, we can easily seal the fracture at both sides and both ends and easily change the contact condition of the fracture. The prepared specimen is shown in Fig.2.

2.2. Procedure of the visualization experiment

The water flooding visualization experiment was carried out on the prepared specimen. In the experiment, the fracture was first saturated with motor oil, and then dyed water was injected into the fracture using a syringe pump under the constant flow rate of 0.2cm^3/min. The small back pressure was applied by adjusting the metering valve set at the outlet. During the flooding experiment, the flow behavior was recorded by a CCD camera. The schematic diagram of the flooding experiment system is shown in Fig.3.

2.3. Results of the visualization experiment

The characteristic four images obtained in the experiment are shown in Fig.4. In these images, the fluid flows from the left to the right. From this figure, it can be observed that injected water does not flow in the whole non-contact areas but it selectively flows in the relatively large apertures and forms clear conduits. This is because the surface of the silicon gum is oil wet, and the water cannot flow in the small apertures without the additional flowing pressure that is greater than the capillary

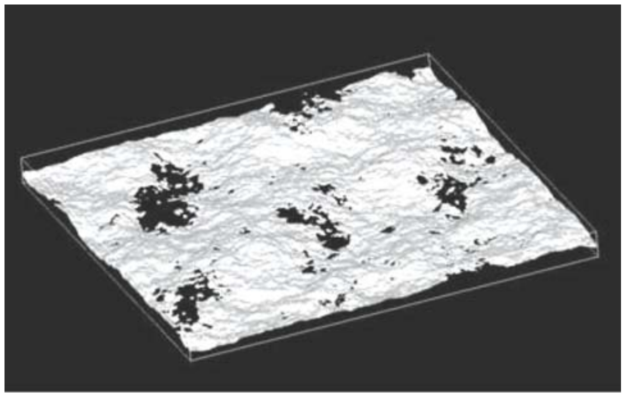

Fig.1. *The numerically generated fracture model using Glover's method*

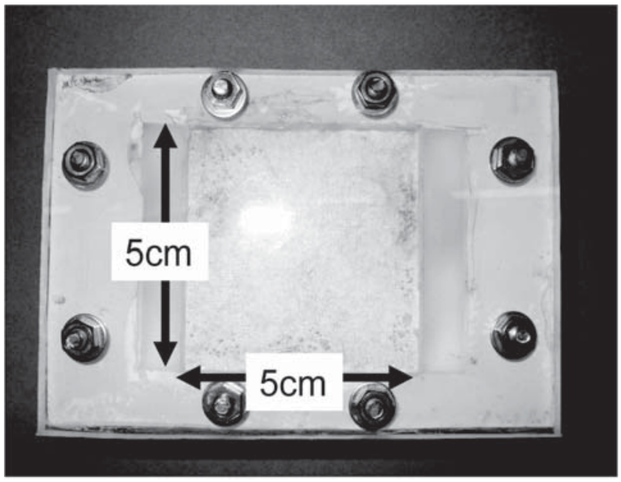

Fig.2. *The specimen for the visualization experiment of water flooding*

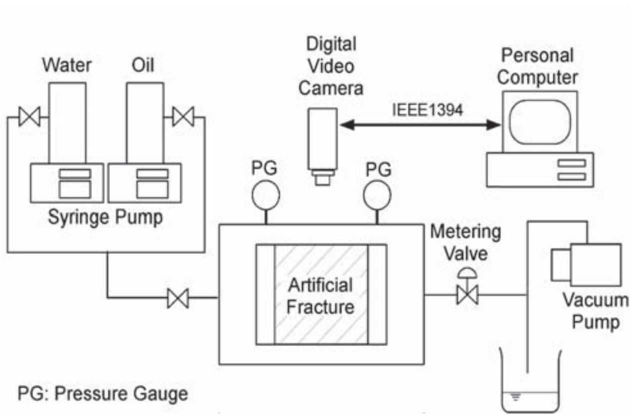

Fig.3. *The schematic diagram of the flooding experiment system*

pressure. The capillary pressure increases with the decrease in the aperture. Furthermore, it can be observed that the conduits cannot develop and the flow reaches a steady state condition after the water break through. This is because the capillary pressure drop occurs in the water phase when the continuous water phase is formed at the water break through, and the flowing pressure in the continuous water phase becomes low after the water break through. The sweep efficiency of this water flooding experiment was 35%.

3. Water flooding simulation in a single fracture by LBM

3.1. Multi-phase LBM

The LBM has succeeded in the flow simulation of complex boundary problem that conventional program codes by Navier-Stokes equation are hard to calculate. It solves a lattice Boltzmann equation for an ensemble-averaged distribution of moving and interacting particles on a discrete lattice. Motion of the particles is limited on the paths connecting the lattice nodes, and all particles on a given path have the same velocity. Interaction of the particles occurs at the lattice nodes by a Boltzmann collision operator. The macroscopic fluid mass and momentum for a given node are obtained by summing the mass and momentum of all particles on the paths emanating from the node. In the LBM, a local equilibrium particle distribution, which determines the Boltzmann collision operator, is assigned so that the macroscopic fluid mass and momentum may satisfy the Navier-Stokes equations.

In order to simulate the immiscible two-phase flow of oil and water, the Boltzmann equation for the colored particles, red (oil) and blue (water) was used in this study. It is given by the following equation.

$$f_i^k\left(\mathrm{x}+\mathrm{c}_i\Delta t, t+\Delta t\right)=f_i^k\left(\mathrm{x}, t\right)+\Omega_i^k\left(\mathrm{x}, t\right) \tag{2}$$

where $f_i^k(\mathrm{x}, t)$ and $\Omega_i^k(\mathrm{x}, t)$ are the particle distribution function and the collision function respectively. They are defined to every kind of particle k, red and blue, and to every direction of particle motion i at the position x and time t. In Equation (2), c_i is the particle velocity in i direction on the lattice, and Δt is the time step during which the particles travel one lattice spacing. The particle velocity vectors on the D3Q15 (3D-LBM with 15 velocities) lattice used in this study is given by

$$\mathbf{c}=\begin{bmatrix} 0 & 1 & 0 & 0 & -1 & 0 & 0 & 1 & -1 & 1 & 1 & -1 & 1 & -1 & -1 \\ 0 & 0 & 1 & 0 & 0 & -1 & 0 & 1 & 1 & -1 & 1 & -1 & -1 & 1 & -1 \\ 0 & 0 & 0 & 1 & 0 & 0 & -1 & 1 & 1 & 1 & -1 & -1 & -1 & -1 & 1 \end{bmatrix} \tag{3}$$

The collision function is decomposed into two terms as Equation (4).

$$\Omega_i^k\left(\mathrm{x}, t\right)=\left(\Omega_i^k\left(\mathrm{x}, t\right)\right)^A+\left(\Omega_i^k\left(\mathrm{x}, t\right)\right)^B \tag{4}$$

The first term of the right side of Equation (4) represents the relaxation from the collision perturbing condition to the local equilibrium condition. This term determines the effect of fluid viscosity in the LBM simulation. The second term represents the surface tension between the two kinds of immiscible fluid.

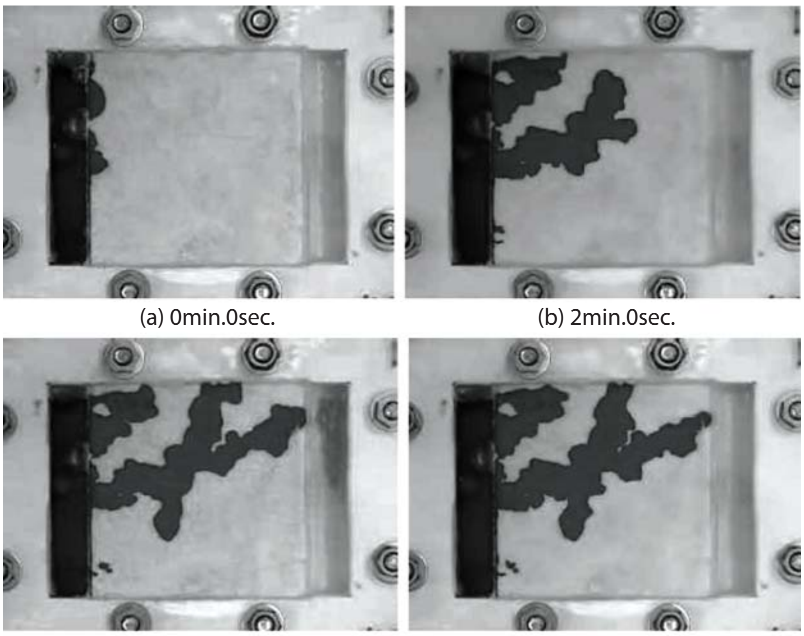

(a) 0min.0sec. (b) 2min.0sec. (c) 2min.43sec. (d) 4min.

Fig.4. *The characteristic images obtained in the water flooding experiment. Water breaks through at 2min. 43 sec., (c)*

The first term of the collision function is defined as Equation (5) applying BGK (Bhatnagar-Gross-Krook) collision operator.

$$\left(\Omega_i^k\left(\mathrm{x}, t\right)\right)^A=-\frac{1}{\tau^k}\left(f_i^k\left(\mathrm{x}, t\right)-f_i^{k(eq)}\left(\mathrm{x}, t\right)\right) \tag{5}$$

where τ^k is the relaxation time to the local equilibrium condition after collision, and $f_i^{k(eq)}$ is the local equilibrium particle distribution function. In this study, in order to get numerical stability, the value of τ^k is set to 1. On the other hand, the second term of the collision function is defined by Equation (6) applying the interfacial tension model proposed by Grunau *et al*[8].

$$\left(\Omega_i^k(\mathbf{x},t)\right)^B = A|\mathbf{F}|\left(\frac{(\mathbf{c}_i\cdot\mathbf{F})^2}{|\mathbf{c}_i|^2|\mathbf{F}|^2}-K\right) \quad (6)$$

where A is the coefficient which controls the magnitude of interfacial tension, and K is the coefficient determined from the mass conservation depending on the lattice model. In this study, A is set to 1.0×10^{-3} for the base case of interfacial tension. K is 1/3 for the 3D15Q lattice model. F is a function called the local color gradient. It is defined by Equation (7).

$$\mathbf{F}(\mathbf{x},t)=\sum_i \mathbf{c}_i\left(\rho_r(\mathbf{x}+\mathbf{c}_i\Delta t,t)-\rho_b(\mathbf{x}+\mathbf{c}_i\Delta t,t)\right) \quad (7)$$

where ρ_r and ρ_b are the density of red fluid and blue fluid respectively. This function has a contribution at the interface of immiscible fluids.

4. Single fracture model used for the simulation

Water flooding simulations were performed to a square single fracture cut out from the single fracture model shown in Fig.1. The size of the single fracture model is 100 lattices in side length and 64 lattices in thickness. As shown in Fig.5(a), 10 lattices in length and 64 lattices in thickness of fluid buffer were added to the both sides of the inlet and outlet. The actual lattices interval is 0.05mm. The aperture distribution is also shown in Fig.5(b). In Fig.5(b), the aperture is shown by the unit length scale of lattice interval. The average aperture of the fracture model is 4.2 lattices and the maximum aperture is 12 lattices. In the both Fig.5(a) and Fig.5(b), one black area is the surface contact area.

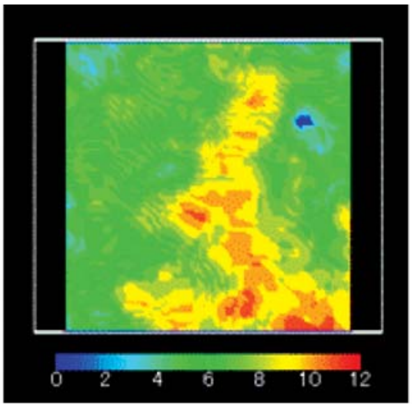

(a)

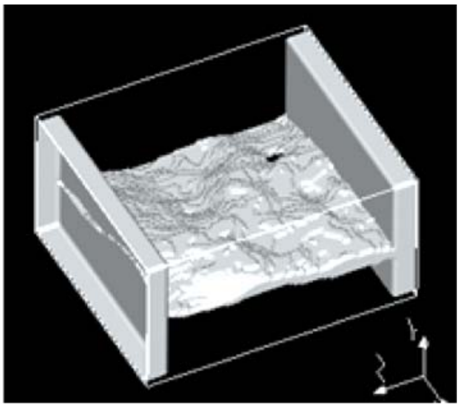

(b)

***Fig.5.** The bird view, (a), and the aperture distribution, (b), of the single fracture model used for the water flooding simulation*

5. Water flooding simulation in a single fracture

In the water flooding simulation, the fracture was perfectly saturated with water at first, and then oil was injected under a constant pressure gradient until irreducible water saturation was accomplished. After that, the water flooding was carried out. In this simulation, the wettability of the fracture surface is perfectly water wet, and the viscosity ratio between oil and water is 4.5. The interfacial tension was set to the base case; A=1.0 x 10^{-3}.

6. Results of the water flooding simulation

The change of the oil saturation is shown in Fig. 6 in the progress of time step. In this figure, the surface contact area and the water saturated areas are indicated by black and blue respectively, and the oil is indicated by the gradation of green color according to its saturation. The deeper green indicates higher oil saturation, and the lighter green indicates lower oil saturation. From this Figure and Fig.5(b), the following are observed. First, oil does not saturate the whole fracture especially the small apertures.

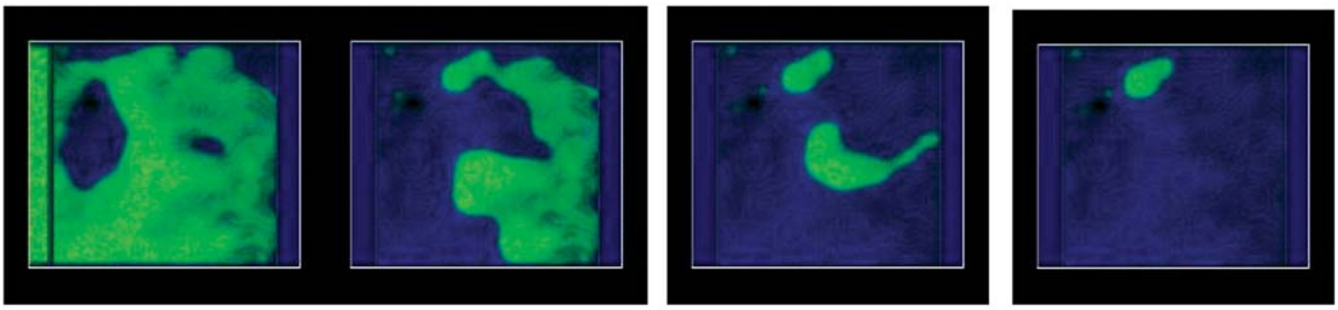

initial *10,000 steps* *20,000 steps* *50,000 steps*

***Fig.6.** The change of the oil saturation observed in the water flooding simulation under the perfectly water wet, the base case of the interfacial tension, and the viscosity ratio of 4.5. The oil is indicated by the gradation of green color according to its saturation*

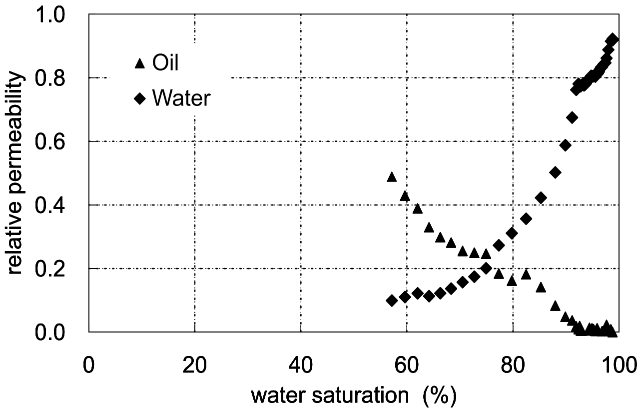

***Fig.7.** The facture relative permeability curves of oil and water obtained from the water flooding simulation*

The initial water saturation is 49.5% as the result. Second, water flows even into the small apertures avoiding the oil saturated large apertures. Some independent oil islands are formed as the result and they are flooded out discontinuously. The residual oil saturation is finally 1.7%. These fluid flow behavior would be caused by the perfectly water wet state of the fracture surface.

7. Relative permeabilty of single fracture

7.1. Relative permeabilty estimation

The relative permeability of the single fracture model was estimated from the average flux of each phase and the water saturation obtained from the water flooding

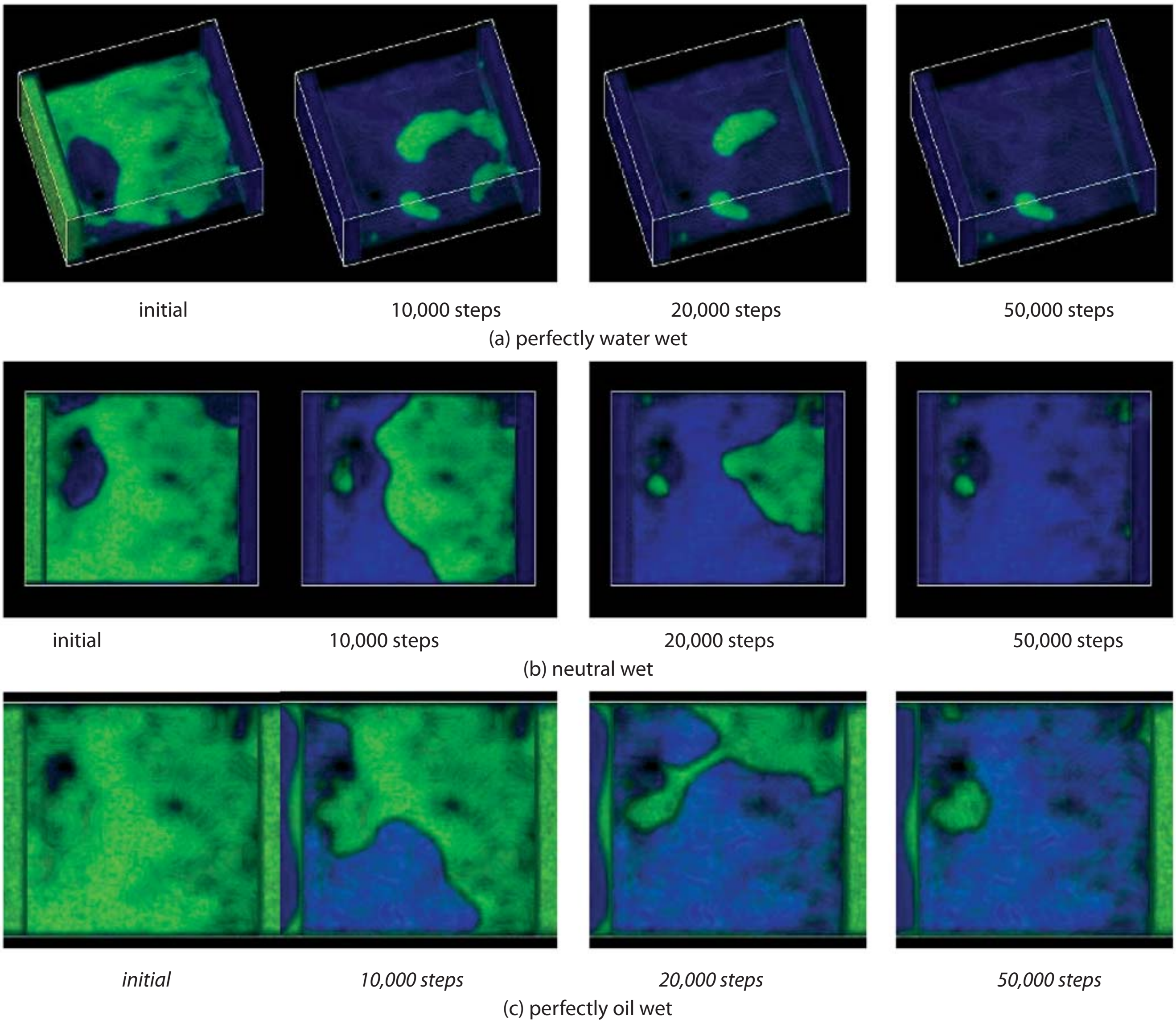

***Fig.8.** The change of the oil saturation observed in the water flooding simulation with changing the wettability to the perfectly water wet (a), the neutral wet (b) and the perfectly oil wet, (c). The oil is indicated by the gradation of green color according to its saturation*

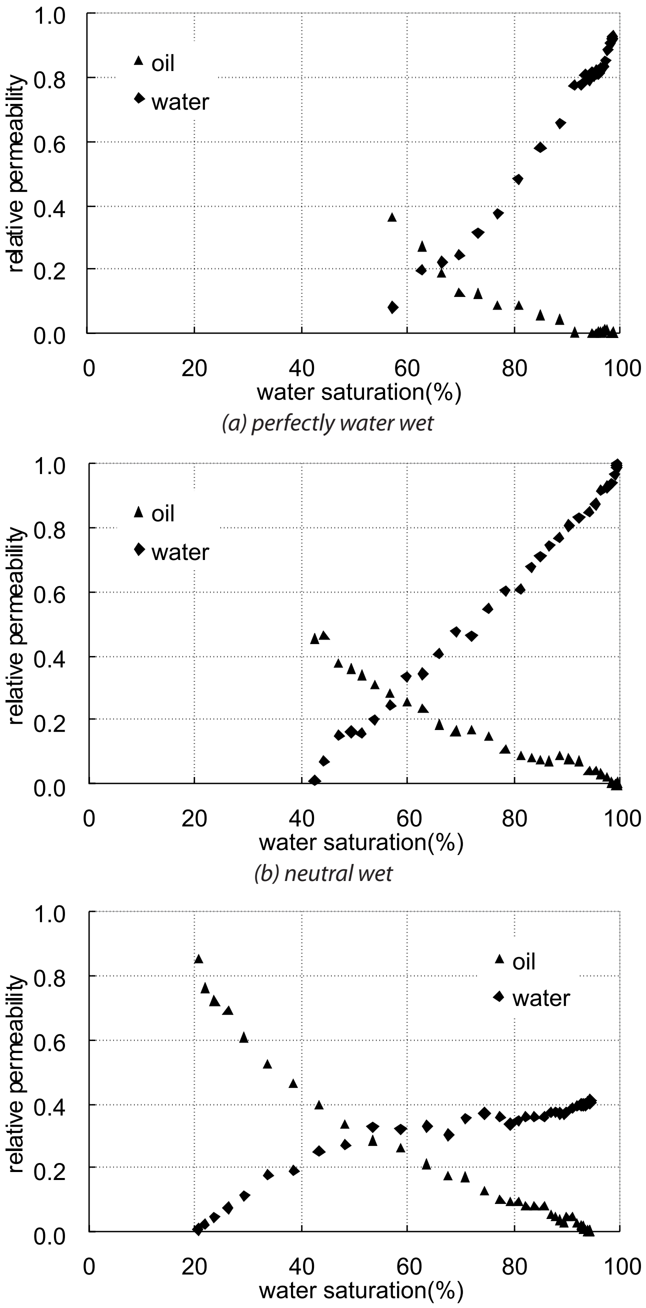

(a) perfectly water wet

(b) neutral wet

(c) perfectly oil wet

Fig.9. *The relative permeability to the three cases of the wettability, (a) perfectly water wet, (b) neutral wet, and (c) perfectly oil wet*

simulation mentioned above. To oil and water, the relative permeability curves concaving downward are obtained as shown in Fig.7. It can be recognized that the relative permeability curves of a single fracture are not straight lines satisfying the relation of $k_{r,nw}+k_{r,w} = 1$. This is probably because each phase of fluid flows are avoiding or pushing each other in the complex aperture distribution of the fracture, and the flow pass consequently becomes as tortuous as the porous reservoir rocks.

7.2. Effect of wettability on relative permeability

The relative permeability would be affected by the wettability and the topography of the fracture surface, the property of aperture distribution, the interfacial tension between oil and water, and the viscosity ratio of the oil viscosity to the water viscosity. Among these affecting factors, the effect of the wettability was first investigated.

Water flooding simulations were performed to the perfectly water wet, the neutral wet, and the perfectly oil wet for the same single fracture model as mentioned above. However, the viscosity ratio is set to one in order to diminish the effect of viscosity. The initial water saturation is 57.2% to the water wet, 42.6% to the neutral wet, and 20.7% to the oil wet. From this initial water saturation condition, water was injected into the fracture under the constant pressure gradient.

The change of the oil saturation is shown in Fig.8 to each case of the wettability in the progress of time steps. In the case of the perfectly water wet, Fig.8(a), the aspect of the flooding is the same as above mentioned although the viscosity ratio is different. The residual oil saturation is 1.5%. In the case of the neutral wet, Fig.8(b), the oil is flooded out continuously without forming the independent oil islands. The residual oil saturation is 0.74%. In the case of the perfectly oil wet, Fig.8(c), the water flows selectively to the large apertures. Two flow paths are formed as the result of avoiding the surface contact area, and the two flow paths surround the small apertures around the surface contact area. The oil in those small apertures is finally left. The residual oil saturation is 5.7% that is the highest among the three cases of wettability.

The relative permeability curves are shown in Fig.9 for each case of wettability. In the case of the perfectly water wet, the water relative permeability is difficult to increase during the small water saturation, because the water flows by avoiding the oil occupying large apertures. But it increasingly increases with the increase in the water saturation, as the water flows through almost the whole fracture. Consequently, the water relative permeability curve concaves downward. In the case of the neutral wet, both relative permeability curves of oil and water become almost straight lines. This is because each phase of the fluid can flow without capillary force. In the case of the perfectly oil wet,

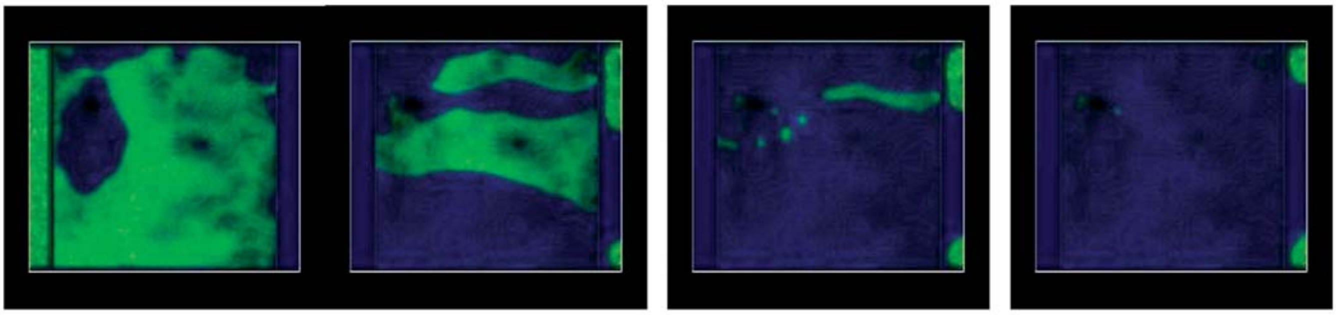

initial *10,000 steps* *20,000 steps* *50,000 steps*

(a) perfectly water wet

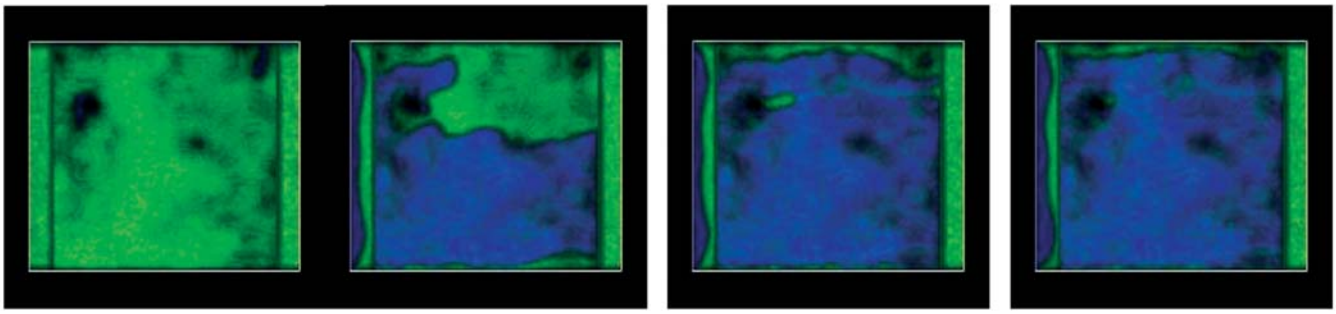

initial *10,000 steps* *20,000 steps* *50,000 steps*

(b) perfectly oil wet

Fig.10. *The change of the oil saturation observed in the water flooding simulation with changing the interfacial tension to 1/10 of the base case for the case of perfectly water wet (a) and the perfectly oil wet (b)*

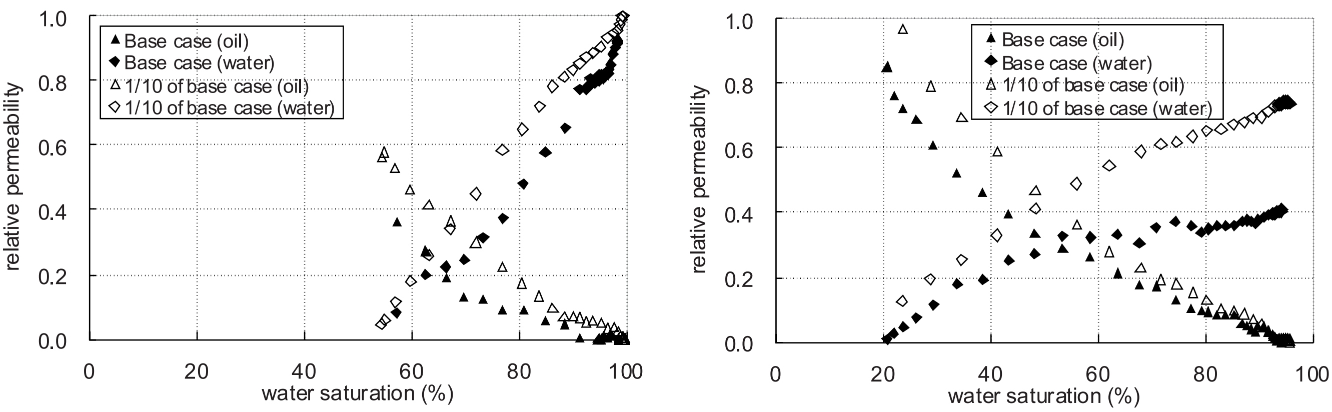

(a) perfectly water wet *(b) perfectly oil wet*

Fig.11. *The change of the relative permeability with the change of the interfacial tension for the case of the perfectly water wet (a) and the perfectly oil wet (b)*

the relative permeability curve concaving upward is obtained. This is because the water flows selectively to the large apertures at first and then it spreads into the small apertures. The flow rate of the water decreases as the result.

7.3. Effect of interfacial tension on relative permeability

The effect of the interfacial tension on the relative permeability was then investigated. We set the value of interfacial tension controlling coefficient, *A*, 1/10 of the base case, and performed the water flooding simulation to the cases of perfectly water wet and perfectly oil wet. The pressure gradient and viscosity ratio are the same as the previous simulations.

The change of the oil saturation is shown in Fig.10 for each case of the wettability in the progress of time steps. Although the flow pattern of both cases of the wettability is almost the same with the base case of the interfacial tension, the residual oil islands become smaller in the case of the perfectly water wet and the water flows into the smaller apertures in the case of the perfectly oil wet by reducing the interfacial tension. The residual oil saturation decreases in the both cases of the wettability. The residual oil saturation is 0.04% for the perfectly water wet and 4.2% for the perfectly oil wet.

The relative permeability curves are shown in Fig.11 for each case of the wettability. In the both cases of wettability, the relative permeability curves approach a straight line. This is probably because the capillary effect becomes small and the flow behavior of the both fluids becomes independent of the aperture distribution.

Conclusions

The water flooding behavior in a single fracture having a complex surface topography are well understood by the visualization experiment and the multi-phase LBM simulation. Moreover, the relative permeability of oil and water for a single fracture is estimated well by the water flooding simulation using the LBM.

From this study, it has been confirmed that the fracture relative permeability curves of oil and water are not straight lines but are curves whose shapes depend on the wettability of the fracture surface and the interfacial tension between oil and water. The water relative permeability curve is concave downward when the wettability is perfectly water wet, the relative permeability curves are almost straight lines when the wettability is neutral wet, and the water relative permeability curve is concave upward when the wettability is perfectly oil wet. Furthermore, the relative permeability curves approach a straight line regardless of the wettability when the interfacial tension between oil and water is reduced.

Some causes of these aspects of the fracture relative permeability have been discussed in this study, but some additional simulation studies for the other conditions of the fracture are necessary to enable more detailed discussions about the affecting factors of the relative permeability.

Acknowledgement

This study was financially supported by JOGMEC as an offered research project from universities in 2006.

References

1. W. R.Rossen and A. T. K.Kumar. *Single- and two-phase flow in natural fractures*. Proc. of the 67th SPE ATC, paper SPE-24195. 1992.

2. P.Persoff and K.Pruess. *Two-phase flow visualization and relative permeability measurement in natural rough-walled rock fractures*. Water Resour. Res. 1995; 31(5), p. 1175 - 1186.

3. T.Iwai, and H.Tosaka. *Laboratory measurement of relative permeability of air-water two-phase flow in a single fracture (in Japanese)*. Shigen-to-Sozai. 2003; 119. p. 593 - 598.

4. N.Speyer, K.Li and R.Horne. *Experimental measurement of two-phase relative permeability in vertical fractures*. Proc. of 32nd workshop on geothermal reservoir engineering Stanford University, SGP-TR-183. 2007.

5. S.R.Brown and C.H.Scholz. *Broad bandwidth study of the topography of natural rock surfaces*. J. Geophys. Res. 1985; 90, p. 12575 - 12582.

6. W. L.Power and T. E.Tullis. *Euclidean and fractal models for the description of rock surface roughness*. J. Geophys. Res. 1991; 96, p. 415 - 424.

7. P.W.Glover, K.Matsuki, R.Hikima and K.Hayashi. *Fluid flow in fractally rough synthetic fractures*. Geophys. Res, Lett. 1997; 24, p. 1803 - 1806.

8. D.Grunau, S.Chen and K.Eggert. *A lattice Boltzmann model for multiphase fluid flows*. Phys. Fluids A. 1993; 5(10): p. 2557 - 2562.